Available online at www.sciencedirect.com
ScienceDirect
Nuclear Instruments and Methods in Physics Research A 584 (2008) 304–318
NUCLEAR INSTRUMENTS & METHODS IN PHYSICS RESEARCH Section A
www.elsevier.com/locate/nima

Comparison of high-energy hadronic shower profiles measured with scintillation and Cherenkov light

N. Akchurin[a], K. Carrell[a], H.P. Paar[b], K.Z. Gümüş[a], J. Hauptman[c], H. Kim[a], O. Lobban[d], A. Penzo[e], R. Wigmans[a,*]

[a]*Texas Tech University, Lubbock, USA*
[b]*University of California at San Diego, La Jolla, USA*
[c]*Iowa State University, Ames, USA*
[d]*St. Mary's University, San Antonio, USA*
[e]*INFN Trieste, Italy*

Received 11 September 2007; received in revised form 8 October 2007; accepted 9 October 2007
Available online 18 October 2007

Abstract

Results are presented of measurements of high-energy hadronic shower profiles with a copper-based fiber calorimeter. This calorimeter was equipped with a mixture of scintillating fibers and undoped (quartz or plastic) fibers. The latter measured the spatial distribution of shower particles with velocities above the Cherenkov threshold, whereas the scintillating fibers measured the distribution of the deposited energy. Both the lateral and longitudinal characteristics of these profiles were measured for pions, with energies ranging from 20 to 300 GeV. The scintillator and Cherenkov profiles exhibit some striking differences, which are discussed and compared with results of Monte Carlo simulations.

PACS: 29.40.Ka; 29.40.Mc; 29.40.Vj

Keywords: Calorimetry; Hadronic shower profiles; Cherenkov light; Optical fibers

1. Introduction

The DREAM calorimeter was developed in the context of a generic R&D project, as a device that would make it possible to perform high-precision measurements of hadrons and hadron jets, while not subject to the limitations imposed by the requirements for compensating calorimetry [1]. The detector is based on a copper absorber structure, equipped with two types of active media which measure complementary characteristics of the shower development. Scintillating fibers measure the total energy deposited by the shower particles, while Cherenkov light is only produced by the charged, relativistic shower particles. Since the latter are almost exclusively found in the electromagnetic (em) shower component (dominated by π^0s produced in hadronic showers), a comparison of the two signals makes it possible to measure the energy fraction carried by this component, f_{em}, event by event. As a result, the effects of fluctuations in this component, which are responsible for all traditional problems in non-compensating calorimeters (non-linearity, poor energy resolution, non-Gaussian response function), can be eliminated. This leads to an important improvement in the hadronic calorimeter performance. The performance characteristics of this detector are described elsewhere [2–4].

The average shower shapes, longitudinal and lateral, have been measured by many groups, both for electromagnetic and hadronic showers, for a variety of absorber materials and particle energies. For example, radial profiles at energies ranging from 10 to 150 GeV were measured by Acosta et al., both for electromagnetic and hadronic

*Corresponding author. Fax: +1 806 742 1182.
E-mail addresses: wigmans@ttu.edu, Richard.Wigmans@ttu.edu (R. Wigmans).

0168-9002/$ - see front matter © 2007 Elsevier B.V. All rights reserved.
doi:10.1016/j.nima.2007.10.015

showers in a lead/scintillating-fiber calorimeter [5]. The longitudinal development of high-energy hadron showers was measured, among others, by Abramowicz et al. [6] and by Catanesi et al. [7]. Amoral et al. [8] measured both the lateral and longitudinal shower development in the ATLAS hadron calorimeter.

Our measurements offer the unique opportunity to compare the shower profiles measured with the relativistic shower particles (through the production of Cherenkov light) with those obtained from energy deposit measurements (scintillation), in otherwise identical experimental conditions. As it turns out, there are some striking differences between these profiles, which have consequences for the calorimetric measurements. In an earlier paper, we have studied these differences, and their effects, for electromagnetic showers [9]. In the present paper, we analyze the profiles of showers induced by high-energy hadrons, i.e., pions.

In Sections 2 and 3, the calorimeter and the experimental setup in which it was tested are described. In Section 4, the experimental data that were taken and the methods used to analyze these data are discussed. In Section 5, the peculiarities of the response of a Cherenkov fiber calorimeter are illustrated with some Monte Carlo results. Experimental results obtained from various data analyses are described and discussed in Section 6. These include longitudinal and lateral hadronic shower profiles measured with scintillation light and Cherenkov light. Differences between the results obtained with the two types of signals are emphasized. A summary and conclusions are presented in Section 7.

2. The DREAM detector

The measurements described in this paper were performed with a calorimeter that has become known by its acronym DREAM (Dual-REAdout Module). The basic element of this detector (see Fig. 1) is an extruded copper rod, 2 m long and $4 \times 4\,mm^2$ in cross-section. This rod is hollow, the central cylinder has a diameter of 2.5 mm. Seven optical fibers are inserted in this hole. Three of these are plastic scintillating fibers,[1] the other four fibers are undoped fibers, intended for detecting Cherenkov light. We used two types of fibers for the latter purpose. For the central region of the detector (Towers 1–7, see Fig. 2), high-purity quartz fibers[2] were used, while the peripheral regions of the detector (Towers 8–19, see Fig. 2) were equipped with acrylic plastic fibers.[3] The latter fibers were considerably cheaper and had a larger numerical aperture (NA) than the quartz ones. Relevant fiber properties are summarized in Table 1.

[1]SCSF-81J, produced by Kuraray Co. Ltd, Tokyo, Japan.

[2]Polymer-clad fused silica fibers, produced by Polymicro, Phoenix, Arizona, U.S.A.

[3]Raytela PJR-FB750, produced by Toray, Japan.

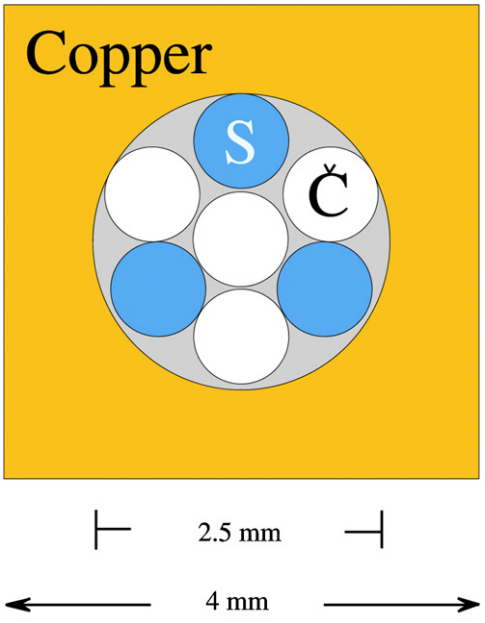

Fig. 1. The basic building block of the DREAM detector is a $4 \times 4\,mm^2$ extruded hollow copper rod of 2 m length, with a 2.5 mm diameter central hole. Seven optical fibers (four undoped and three scintillating fibers) with a diameter of 0.8 mm each are inserted in this hole, as shown.

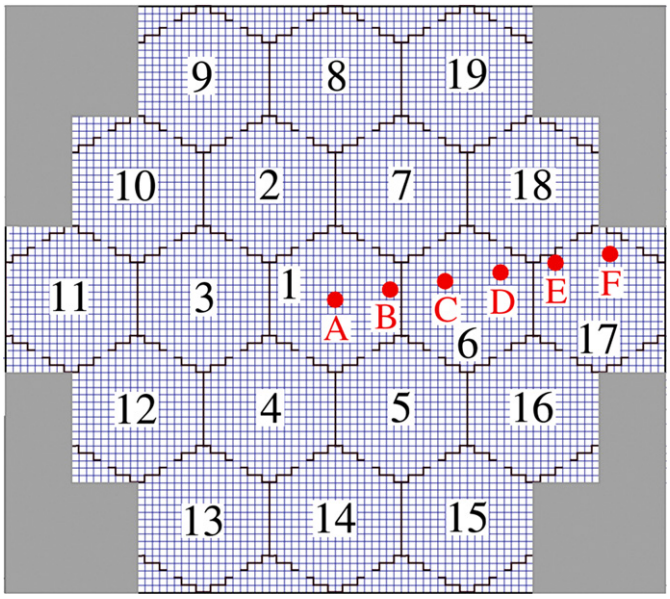

Fig. 2. Schematic layout of the DREAM calorimeter (front view). Each square represents a copper tube, shown in detail in Fig. 1. The subdivision into (numbered) hexagonal readout towers is shown, as well as the impact points (*A–F*) of the particles used for the lateral profile studies.

The fiber pattern was the same for all rods, as shown in Fig. 1. The DREAM detector consists of 5580 such rods, 5130 of these are equipped with fibers. The instrumented volume thus has a length of 2.0 m, an effective radius of $\sqrt{5130 \times 0.16/\pi} = 16.2\,cm$ and a mass of 1030 kg. The effective radiation length (X_0) of the calorimeter amounts to 20.10 mm, the Molière radius (ρ_M) is 20.35 mm and the nuclear interaction length (λ_{int}) 200 mm. The composition

Table 1
Properties of the fibers used in this experiment

Fiber type	Light source	n_{core}	N.A.	λ_{att} (m)
SCSF-81J	Scintillation	1.59	0.72	5[a]
Quartz	Cherenkov	1.458	0.33	15
Clear plastic	Cherenkov	1.49	0.50	8

Listed are for each type of fiber, the light source responsible for the signals, the index of refraction of the fiber core material (measured at 500 nm), the numerical aperture and the attenuation length. The fibers were polished on both ends, no reflective material was used. The fibers were separated by a 1–2 mm thick air gap from the PMTs.

[a]Measured with a yellow filter (Kodak Wratten #3) between fibers and PMT.

of the calorimeter is as follows: 69.3% of the detector volume consists of copper absorber, while the scintillating and Cherenkov fibers occupy 9.4% and 12.6%, respectively. Air accounts for the remaining 8.7%. Given the specific energy loss of minimum ionizing particles (mips) in copper (12.6 MeV/cm) and polystyrene (2.00 MeV/cm), the sampling fraction of the copper/scintillating-fiber structure for mips is thus 2.1%.

The fibers were grouped to form 19 towers. Each tower consists of 270 rods and has an approximately hexagonal shape (80 mm apex to apex). The effective radius of each tower is 37.1 mm ($1.82\rho_M$). A central tower (#1) is surrounded by two hexagonal rings, the Inner Ring (6 towers, numbered 2–7) and the Outer Ring (12 towers, numbered 8–19). The towers are longitudinally unsegmented. The readout structure is shown schematically in Fig. 2.

The depth of the copper structure is 200 cm, or $10.0\lambda_{int}$. The fibers sticking out at the rear end of this structure were separated into 38 bunches: 19 bunches of scintillating fibers and 19 bunches of Cherenkov fibers. In this way, the readout structure was established. Each bunch was coupled through a 2 mm air gap to a photomultiplier tube (PMT).[4] More information about this detector is given elsewhere [2,3].

3. Experimental setup

3.1. The beam line

The measurements described in this paper were performed in the H4 beam line of the Super Proton Synchrotron at CERN. The DREAM detector was mounted on a platform that could move vertically and sideways with respect to the beam. Changing the angle of incidence of the beam particles with respect to the fibers in the horizontal plane (the ϕ angle) and the tilt angle (θ) was achieved with the intervention of a crane. For the measurements described in this paper, we used three different detector orientations:

(Π) Lateral profiles were obtained from measurements in which the angles ϕ and θ were both 0. The beam particles thus entered the detector perpendicular to its front face, parallel to the fiber axes. Six different impact points were used for these measurements (see Fig. 2).

(Δ) For the longitudinal profiles, the detector was rotated over an angle in the horizontal plane. Most data were taken at ($\phi = 24^\circ$, $\theta = 0$), where the beam entered the detector in Tower 17, as indicated in Fig. 3. This orientation was chosen since it allowed a measurement of the longitudinal shower profiles over a depth of almost 1 m ($4.5\lambda_{int}$).

(Γ) In a subsequent test period, the detector was rotated to the position ($\phi = 90^\circ$, $\theta = 0$), with the beam entering the detector in Tower 11, as indicated in Fig. 3. In this case, the detector depth was limited to 36 cm ($1.8\lambda_{int}$).

Several auxiliary detectors were used in these beam tests. These detectors served to obtain clean event samples and to measure the impact point of the particles event by event. Two small scintillation counters provided the signals that were used to trigger the data acquisition system. These Trigger Counters were 2.5 mm thick, and the area of overlap was $6 \times 6\,cm^2$. A coincidence between the logic signals from these counters provided the trigger.

The impact point of the beam particles in the DREAM detector was measured with a *fiber hodoscope*. This hodoscope consisted of ribbons of scintillating fibers oriented in the horizontal or vertical direction, thus providing the y and x coordinates of the beam particles. The fibers were 500 μm thick. Their signals were read out by means of multi-anode PMTs. This hodoscope was installed about 3 m upstream of the front face of the DREAM calorimeter. It was possible to determine the coordinates of the impact point in the calorimeter with a precision of a fraction of 1 mm, depending on the energy of the particles. More details about this hodoscope, and examples of its excellent performance, are given in Ref. [2].

The *preshower detector* consisted of a 5 mm thick ($1X_0$) lead absorber, followed by a scintillation counter. This simple device turned out to be extremely useful for eliminating electron contamination [2]. Downstream of the calorimeter, behind an additional $8\lambda_{int}$ worth of absorber, a $30 \times 30\,cm^2$ scintillator paddle served to identify muons that contaminated the pion beams.

3.2. Data acquisition

The various detector signals were transported through RG-58 cables with (for timing purposes) appropriate lengths to the counting room. All signals, except those from the trigger counters and the fiber hodoscope, were digitized by 11-bit LeCroy 2249W charge-sensitive ADCs. These had a gain of 4 counts/pC. The ADC gate width was 120 ns, and the calorimeter signals arrived ~30 ns after the start of the gate. The signals from the fiber hodoscope were digitized by TDCs. Eight TDCs were used, four for the horizontal and four for the vertical fiber ribbons,

[4]Hamamatsu R-580, 10-stage, 1.5 in. diameter.

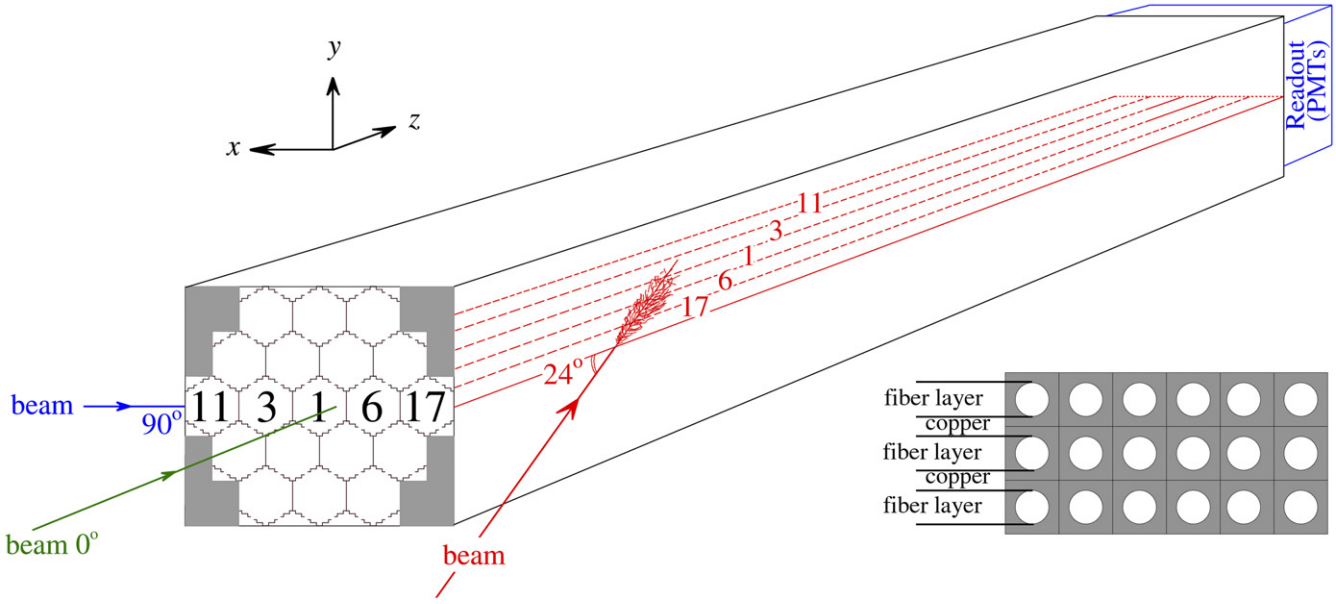

Fig. 3. Orientation of the DREAM calorimeter in positions $\Pi(0,0)$, $\Delta(24^\circ,0)$ and $\Gamma(90^\circ,0)$. The electron beams entered the detector in the horizontal (x–z) plane, at an angle $\phi = 0^\circ$, 24° or 90° with the direction of the fibers (the z-direction). The insert shows the fine-structure of the calorimeter, with horizontal fiber planes separated by layers of copper.

respectively. The time information was converted into the (x, y) coordinates of the point where the beam particle traversed the hodoscope.

The data acquisition system was based on CAMAC, interfaced via a VME bus to a Linux-based computer. A maximum of 2000 events were recorded in the 2.6 s SPS spill. The typical event size was ~150 bytes. All calorimeter signals and the signals from the auxiliary detectors were monitored on-line.

3.3. Calibration of the detectors

Using the high voltage, the gain in all PMTs was set to generate ~4 pC/GeV. The 38 PMTs reading out the 19 towers were calibrated with 40 GeV electrons. The showers generated by these particles were not completely contained in a single calorimeter tower. The (average) containment was found from EGS4 Monte Carlo simulations. When the electrons entered a tower in its geometrical center, on average 92.5% of the scintillation light and 93.6% of the Cherenkov light was generated in that tower [2]. The remaining fraction of the light was shared by the surrounding towers. We assumed the energy sharing to be the same for all towers. The signals observed in the exposed tower thus corresponded to an energy deposit of 37.0 GeV in the case of the scintillating fibers and of 37.4 GeV for the Cherenkov fibers (no difference was observed between towers equipped with plastic fibers and quartz ones). These energy values, together with the precisely measured values of the average signals from the exposed tower, formed the basis for determining the calibration constants, i.e., the relationship between the measured number of ADC counts and the corresponding energy deposit. The stability of the calibration constants was checked four times during the test period by sending 40 GeV electrons into the center of each calorimeter tower and measuring the signal distribution. The mean values of these distributions were stable to within 2% in these measurements, for all 38 channels.

However, fluctuations in the calibration constants resulting from PMT gain variations are not the only source of experimental errors in the energies assigned to the signals. Other sources of systematic errors include:

- Fiber-to-fiber response variations. Laboratory tests of fiber samples with a radioactive source revealed response fluctuations with a σ_{rms} of the order of 10%. Since every high-energy shower signal (even for the narrow em showers) represents the integral over hundreds of fibers, the effects of these fluctuations on the hadronic calorimeter response are negligible.
- Variations in photocathode efficiency over the surface of a given PMT. These translate into an impact point dependence of the calorimeter response. We have measured this effect for the central tower (#1) in some detail, and the results of these measurements are published in Ref. [2]. For em showers, the response variations had a σ_{rms} of 1.8% for the scintillator signals and 3.2% for the Cherenkov signals.
- Temperature and other environmental factors. We did not monitor these.

4. Experimental data

Events were triggered by coincident signals in the scintillation counters upstream of the calorimeter. Only

events for which the (x, y) coordinates of the beam particle in the fiber hodoscope were measured were retained for the analyses. One purpose of the hodoscope information was to be able to limit the impact region of the beam particles. For most of the analyses described in this paper, a circular region with a radius of 1.0 cm was selected.

The following data sets were used for these analyses:

(1) π^- data at 20, 40, 50, 80, 100, 150, 200, 250 and 300 GeV, taken with the detector oriented in position $\Delta(24^\circ, 0^\circ)$. These data were used to measure the longitudinal hadronic shower profiles.
(2) π^+ data at 20, 50, 80, 100, 200 and 300 GeV, taken with the detector oriented in position $\Gamma(90^\circ, 0^\circ)$. These data were used for detailed measurements of the initial stages (i.e., the first $1.5\lambda_{\text{int}}$) of the hadronic shower development.
(3) A scan with 100 GeV π^+ was performed in six steps of $\sim$3 cm, with the calorimeter oriented in position $\Pi(0, 0)$. The impact points used in this scan (A–F) are indicated in Fig. 2. These data were used for measuring the lateral hadronic shower profiles.

For each data point, at least 100 000 events were collected. For some data points, especially at energies $\geqslant$100 GeV, several runs of 100 000 events each were carried out. Pure hadron event samples were obtained using the information from the Preshower Detector and the Muon Counter. The procedures, as well as examples of the results achieved in this context, are described in Ref. [2].

5. Angular dependence of the Cherenkov response

Unlike the scintillator response (or the response of any other active medium measuring $\mathrm{d}E/\mathrm{d}x$ for that matter), the response of a fiber calorimeter based on the detection of Cherenkov light depends on the angle of incidence of the showering particles. This has a number of consequences, some of which were encountered in the present analysis. To illustrate the phenomena that play a role, we show below some results of EGS4 Monte Carlo simulations of *electromagnetic* showers developing in the DREAM calorimeter. These effects have also consequences for the hadronic characteristics studied in this paper.

The angular dependence of the Cherenkov response derives from the fact that the Cherenkov light is emitted at a characteristic angle by the superluminous shower particles, combined with the fact that the angular distribution of these shower particles is non-uniform [10]. Fig. 4 shows the angular distribution of the relativistic charged shower particles (with velocities $\beta > 1/n$) generated by 40 GeV electrons entering the DREAM calorimeter at an angle $\vartheta = 20^\circ$ with the fiber direction. This distribution is weakly dependent on $\cos\vartheta$, except for a sharp peak near $\cos\vartheta = 0.94$ ($\vartheta = 20^\circ$). This peak is due to numerous electrons and positrons produced in the early, collimated part of the shower by conversion of photons radiated by the incoming particle. The other component, which extends all the way to the backward region, is dominated by electrons produced in Compton scattering and the photoelectric effect.

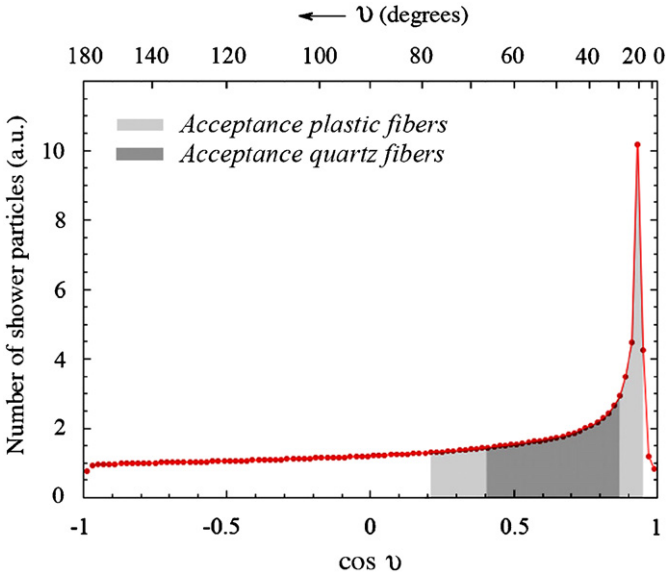

Fig. 4. Angular distribution of the shower electrons and positrons with $\beta > 1/n$, for a 40 GeV electron beam entering the DREAM calorimeter at an angle $\vartheta = 20^\circ$ with the fiber direction. The shaded areas indicate which of these shower particles contribute to the Cherenkov signals registered in the quartz and plastic fibers. Results of EGS4 Monte Carlo simulations. The larger range for the plastic fibers reflects their larger numerical aperture. All angles are measured with respect to the fiber direction.

The shaded areas in Fig. 4 indicate which of these shower electrons and positrons may contribute to the Cherenkov signals from this calorimeter. These are the particles that travel at angles with the fiber axis that fall within the cone defined by the Cherenkov angle and the numerical aperture of the fibers. This cone has an opening angle of $2\arcsin[\mathrm{NA}]$, and its axis makes an angle of $\vartheta_C = \arccos n^{-1}$ with the fiber direction. In the example given here, the Cherenkov light emitted by the shower particles in the forward peak falls within the acceptance of the plastic fibers (NA = 0.5), but outside the acceptance of the quartz fibers (NA = 0.33).

The calorimeter response thus clearly depends on the extent to which the Cherenkov light associated with the forward peak falls within the acceptance of the fibers. This in turn depends, apart from this acceptance, on the angle of incidence of the showering particles [11]. Fig. 5 shows the calorimeter response to 40 GeV electrons as a function of this angle, both for the quartz and the plastic fibers. These results were derived from the distribution shown in Fig. 4 by folding in the energy deposited by each individual shower particle that contributes to the Cherenkov signal.[5]

[5]This figure is only intended to illustrate the effect of the difference in numerical aperture. Details about light transportation in the fibers and transfer to the photocathode, which may affect the precise shape of the angular dependence, were not taken into account in the simulations.

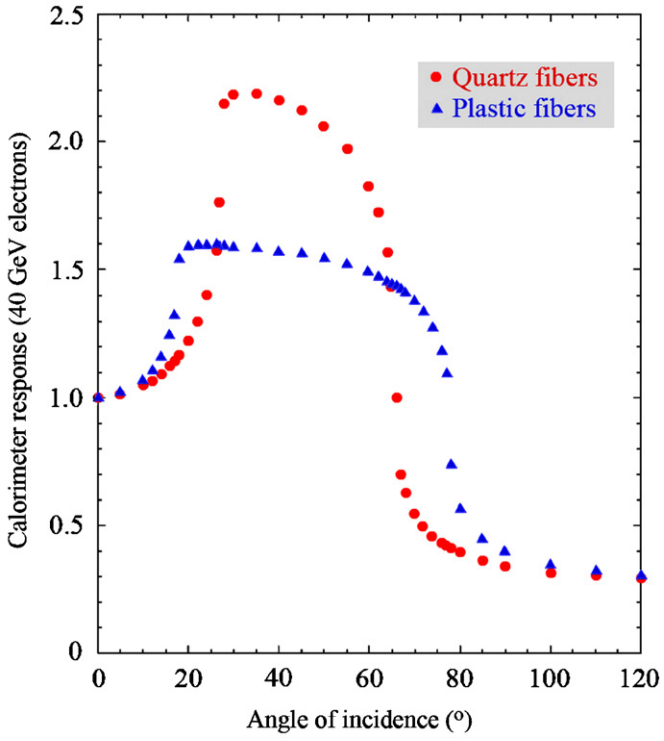

Fig. 5. The response of a DREAM calorimeter equipped with quartz or plastic Cherenkov fibers, as a result of the angle of incidence of the showering (40 GeV) electrons. The response is in both cases normalized to $\vartheta = 0°$, i.e., the electron beam is parallel to the fiber direction. Results of EGS4 Monte Carlo simulations.

The response is equalized for $\vartheta = 0$, the angle at which the different calorimeter cells were calibrated. At this angle, the forward peak does *not* contribute to the signals from either type of fiber. The figure shows that the response initially increases with the angle of incidence, reflecting the fact that the Cherenkov cone associated with the forward peak starts to fall within the numerical aperture, first of the plastic fibers, and at angles larger than $\sim 30°$ also for the quartz fibers. The response reaches a maximum value that is about 2.2 (1.6) times the reference value for the quartz (plastic) fibers. The difference between quartz and plastic derives from the fact that the fraction of the total Cherenkov light in the acceptance cone that is emitted by the Compton electrons is larger for the plastic fibers. Therefore, the inclusion of the forward peak has a relatively smaller effect on the total Cherenkov response than for the quartz fibers.

For angles $\vartheta > 65$–$75°$, the Cherenkov light associated with the forward peak starts to fall outside the numerical acceptance, and Compton electrons are the only source of the signals. At $\vartheta = 90°$, the geometry for which data set 2 was obtained, the response amounts to 34% (40%) of the reference value for the quartz (plastic) fibers. It further decreases for angles beyond 90°.

These results for em showers turned out to be important for understanding some of the peculiarities observed for the signals from hadron showers.

6. Experimental results

All results shown in this section concern *average* shower characteristics. The shower profiles, leakage fractions and signal ratios were averaged over very large event samples, typically 100 000 events per data point. As a result, the experimental uncertainties are usually dominated by systematic effects, since the statistical errors are typically a small fraction of 1%.

6.1. Lateral shower profiles

Lateral shower profiles provide information about the energy deposit characteristics in a plane perpendicular to the shower axis. This information may be integrated over the full depth of the shower development, or it may concern a specific depth segment, e.g., the region around the shower maximum. The lateral profiles derived from our analysis are of the first type, i.e., integrated over the full depth. Since the shower development is, on average, cylindrically symmetric, lateral shower profiles are best described in terms of dE/dr, the energy density as a function of the distance (r) to the shower axis. In that case, they are also called *radial* profiles.

6.1.1. Measurement data

We used the data from the 100 GeV π^+ scan for this study (data set 3, see Section 4). The beam entered the calorimeter in six different locations during this scan (A–F, Fig. 2). For each of these event samples, the distances r_i to the centers of the 19 calorimeter towers were calculated. In total, we thus had signal distributions for $6 \times 19 = 114$ different r_i values.

For each of these signal distributions, we determined the average energy deposit. Since many energy deposits were very small, especially at large distances from the shower axis, the mean value was determined by averaging the number of raw ADC counts for *all* events, and subtracting from this the average pedestal value. The difference was subsequently converted into energy units. This procedure was carried out for all 114 signal distributions, separately for the scintillator and the Cherenkov signals. Fig. 6 shows the r-dependence of the 114 mean values obtained in this way, separately for the scintillator signals and the Cherenkov signals. Fig. 6b includes the signals from both types of Cherenkov fibers.

Proper measurements of radial shower profiles require, ideally, a detector with a cell size (A) that is small compared to the characteristic features of that profile. If the cell size is too large, smearing effects tend to obscure these features. The profiles displayed in Fig. 6 exhibit the same characteristic features as reported in other studies of the lateral development of pion-induced showers [12,5,8], i.e., a rather narrow central core surrounded by a halo that decreases exponentially in intensity. Profiles of this type have been successfully described by the sum of a Gaussian

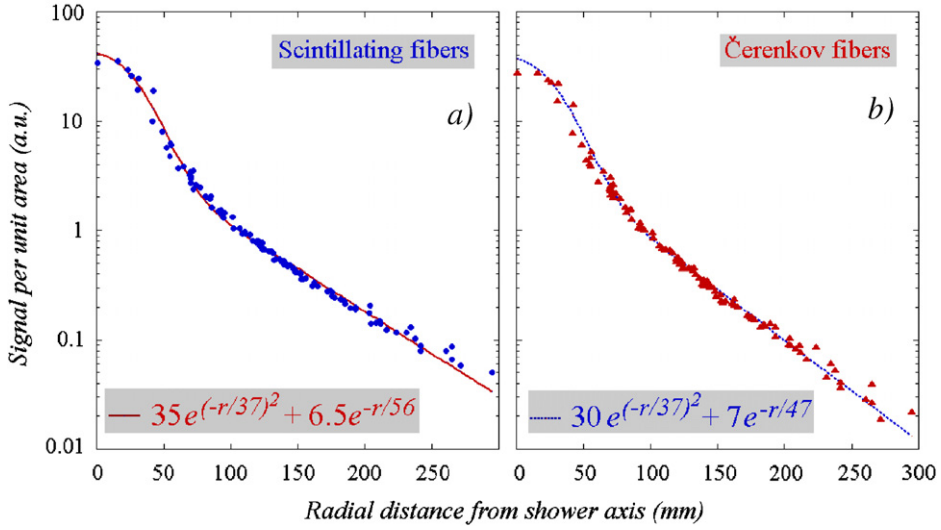

Fig. 6. Measurement of the lateral profile of 100 GeV π^+ showers, obtained by combining event samples from a grid scan. Each point represents the mean value of the signal distribution measured in a tower at a radial distance r from the shower axis. Results are given separately for the scintillator signals (a) and for the Cherenkov signals (b). The curves represent the results of fits to (1).

and an exponential function:

$$\left[\frac{dE}{dA}\right](r) = c_1 e^{-r^2/\lambda_1^2} + c_2 e^{-r/\lambda_2} \quad (1)$$

The curves drawn in Fig. 6 represent the results of fits to a function of this type. Since we are mainly interested in *differences* in lateral shower containment, which are determined by the exponential term, and because of differences between the properties of the two types of clear fibers (discussed below), we decided to use the same value of λ_1 for the Cherenkov profile as found for the scintillator profile. The values of λ_2 were found to be significantly different for the two profiles. The Cherenkov profile decreases more steeply with r ($\lambda_2 = 4.7$ cm) than the scintillator profile ($\lambda_2 = 5.6$ cm).

The *ratio* of the average Cherenkov and scintillator signals is shown as a function of the radial distance r in Fig. 7. We have distinguished the data points for towers equipped with quartz fibers (Towers 1–7, see Fig. 2) from those for the towers equipped with clear plastic fibers (Towers 8–19). The distributions look quite different for these two data sets, despite the relatively large point-to-point spread in the signal ratio, which reflects the very small number of photoelectrons that characterized the Cherenkov signals, typically only 500 *for the entire* 100 GeV π^+ *shower*. In the case of the plastic fibers, the ratio of the Cherenkov and scintillator signals steadily decreases as we move away from the shower axis. In the case of the quartz fibers, this effect is much smaller, if present at all.

The reason for this difference is the different numerical aperture of the two types of fibers (0.33 for quartz, 0.50 for plastic). As we look at the signals generated at a certain distance from the shower axis, the average angle between the shower particles and the direction of the fibers changes. The larger the distance between the tower and the shower axis, the larger this angle becomes. This is particularly true for the π^0s produced in the nuclear reactions. These π^0s produce em showers and dominate the Cherenkov signals from hadron showers in this type of calorimeter. As illustrated in Fig. 5, the calorimeter response increases when the angle between the π^0s and the fiber axis gets different from (i.e., larger than) zero. For angles larger than ~20°, this effect is considerably larger for the quartz fibers than for the plastic ones.

The change of the measured Cherenkov/scintillator signal ratio as a function of the radial distance r is thus the result of two competing effects:

(1) A genuine decrease of the ratio of Cherenkov and scintillation photons, which is the result of the fact that the em shower component is more concentrated around the shower axis than the halo of non-relativistic shower particles (mainly protons) which do generate scintillation, but no Cherenkov signals.
(2) An increase in the fraction of the Cherenkov photons that are emitted within the numerical aperture of the fibers and thus contribute to the Cherenkov signals.

For reasons discussed above, the offsetting effect of the latter increase is larger in the case of the quartz fibers. Therefore, the profiles in Figs. 7a and b are significantly different. Nevertheless, Fig. 7a makes it very clear that the radial shower profiles (i.e., the photon density as a function of r) of 100 GeV pions are significantly different for the two types of signals. In particular, the Cherenkov signals are much more concentrated in a region near the shower axis than the scintillator signals.

6.1.2. *Lateral shower containment*

The parameterized radial profiles can be used to estimate the lateral containment of the 100 GeV pion showers, and

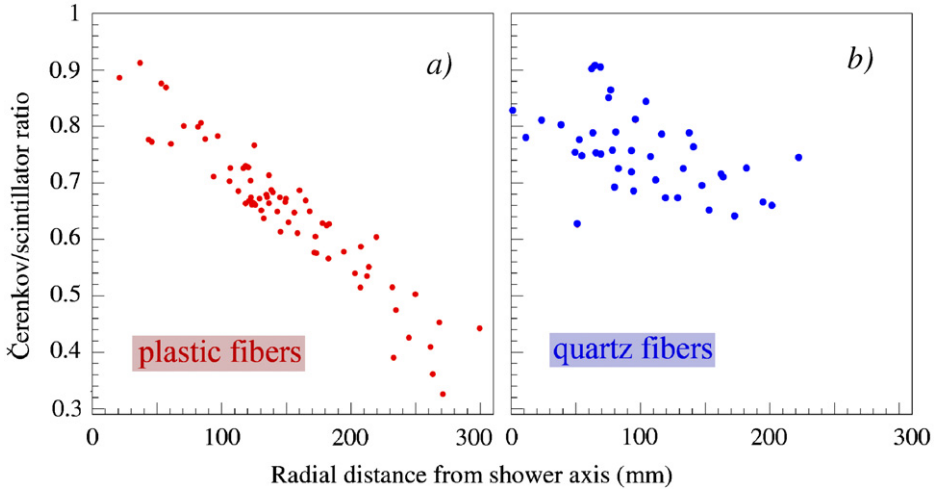

Fig. 7. Measurement of the lateral profile characteristics of 100 GeV π^+ showers, obtained by combining event samples from a grid scan. Each point represents the ratio of the mean values of the Cherenkov and scintillator signal distributions measured in a tower at a radial distance r from the shower axis. Results are given separately for the Cherenkov signals measured with the clear plastic fibers (a) and with the quartz fibers (b). See text for details.

thus the shower leakage. The average energy fraction leaking out of a cylinder with radius r_0 around the shower axis was calculated as follows:

$$f_{\text{leak}} = \frac{\int_{r_0}^{\infty} r[\mathrm{d}E/\mathrm{d}A](r)\,\mathrm{d}r}{\int_{0}^{\infty} r[\mathrm{d}E/\mathrm{d}A](r)\,\mathrm{d}r} \quad (2)$$

where $\mathrm{d}E/\mathrm{d}A(r)$ is given by Eq. (1). Since the Gaussian component of this equation describes the profile close to the shower axis, the leakage for $r \gtrsim 100$ mm is completely determined by the properties of the exponential component. For the Cherenkov signals, this exponential component is mainly determined by the signals from the towers equipped with plastic fibers, since these were, on average, located farthest from the shower axis. The leakage fraction is shown as a function of r_0 in Fig. 8, for the two types of calorimeter signals. For a given detector size, the containment is systematically larger when the Cherenkov signals are used. For example, when 100 GeV pions entered the DREAM calorimeter in its central region, on average, 9.7% of the total amount of scintillation light they could generate in an infinitely large instrument of this type escaped the 19-tower detector, vs. 5.9% of the Cherenkov light. These numbers were calculated by approximating the lateral cross-section of the DREAM calorimeter (see Fig. 2) with a circle of the same surface area ($r_0 = 16.2$ cm). Fig. 8 also shows that in order to contain on average 99% of the light, the radial size of the DREAM calorimeter would have to be increased to 26 cm for the Cherenkov light and 32 cm for the scintillation light.

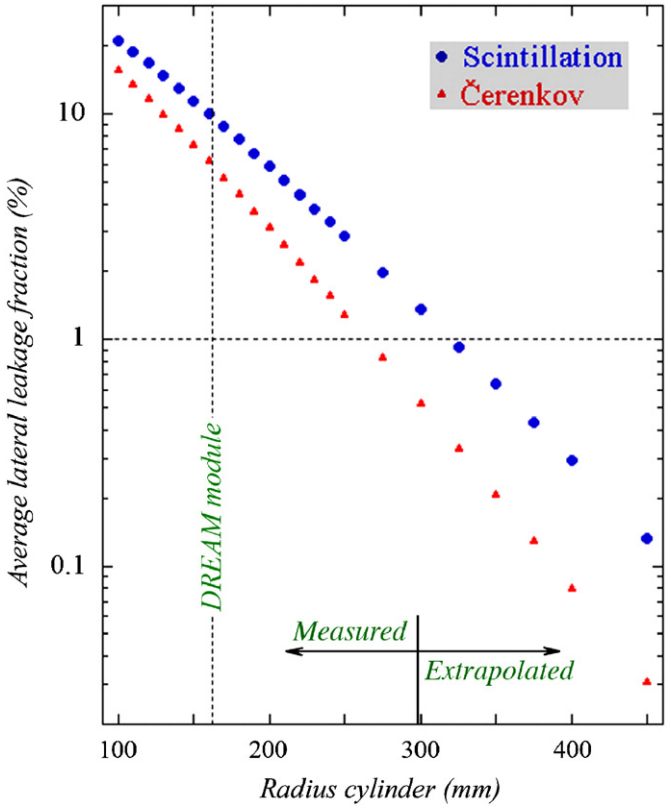

Fig. 8. Leakage outside of a DREAM calorimeter cylinder, as a function of the radius of that cylinder. Results are given as a fraction of the total signal in an infinitely large calorimeter, separately for scintillation and Cherenkov light.

6.1.3. Comparison with other experiments

Measurements of lateral hadronic shower profiles have been performed by a variety of other groups. Some groups have also measured these profiles at various stages of the shower development, e.g., ZEUS [12] and ATLAS [8]. Others have performed detailed measurements of the integrated shower profile [5]. In these examples, the cell size was considerably larger than in our case, and some authors have undertaken elaborate attempts to unfold the underlying shower profile. A detailed comparison of the various results is complicated by the fact that different parameterizations are being used. For example, [8] used a

sum of three exponentials, [13] a sum of two exponentials, [14] a sum of two exponentials with energy dependent decay constants and [5] the sum of a Gaussian and an exponential. Our goal was primarily to study *differences* between the profiles measured with scintillation and Cherenkov light. These differences manifest themselves at relatively large distances from the shower axis. Therefore, we did not make efforts to extract details of the profiles close to the shower axis, which would have required a very different (event-by-event) approach, since the size of the beam spot was not negligible compared to that of the central core of the profile.

Nevertheless, it is possible to compare some of our results with those from the mentioned other studies, in particular the radial detector dimensions needed for certain levels of shower containment. Table 2 lists the detector radii needed for 95% and 99% containment for a number of calorimeters, of which the composition is given in the second column. Not all measurements were performed at the same energy, which should be kept in mind since the average shower profile tends to become more concentrated around the shower axis as the energy increases, due to the increased value of the average em shower fraction. The containment results obtained in our study for the scintillation light are, both at the 95% and the 99% level, almost identical to those in the ATLAS [8] and IILC [14] hadron calorimeters, when the dimensions are expressed in terms of λ_{int}. Remarkably, the cylinder has to be much larger when lead [5] or uranium [12] is used as absorber material, instead of iron or copper. This is most likely due to the dominant contribution of neutrons to the signals from these lead and uranium calorimeters. The characteristic length scale for that particular shower component is *not* the nuclear interaction length.

We are only aware of one hadronic shower profile measurement in a Cherenkov-based calorimeter [13]. However, in this case the measurements extended radially only up to 10 cm from the shower axis. Therefore, it was not possible to estimate $r_{99\%}$ with adequate precision. The value of $r_{95\%}$ is somewhat smaller than that derived in the present study. However, it does confirm our observation that hadronic showers measured in a Cherenkov calorimeter appear to be considerably more narrow than in a calorimeter based on $\mathrm{d}E/\mathrm{d}x$.

Table 2
The radial detector size needed to contain 95% and 99% of the light signals generated in the shower development, for different calorimeters

Experiment	Calorimeter	Energy (GeV)	$r_{95\%}$ (λ_{int})	$r_{99\%}$ (λ_{int})
ATLAS [8]	Fe/scintillator	100	1.04	1.67
IILC [14]	Fe/scintillator	100	1.18	1.68
SPACAL [5]	Pb/scintillator	80	1.52	2.7
ZEUS [12]	^{238}U/scintillator	100	2.1	3.0
CMS QFCAL [13]	Cu/quartz[a]	80	0.65	
This experiment	Cu/scintillator	100	1.06	1.60
This experiment	Cu/clear plastic	100	0.86	1.30

The calorimeters are assumed to be infinitely deep, so that longitudinal leakage plays no role.

[a]Measurements extended only over 10 cm. Therefore impossible to determine $r_{99\%}$.

6.2. Longitudinal shower profiles

Longitudinal shower profiles were obtained from the energy sharing between the different calorimeter towers in the two geometries depicted in Fig. 3, in which the beam pions entered the detector at 24° and 90° with the fiber direction, respectively (data sets 1 and 2, see Section 4).

Inspection of the 24° geometry shows that the showering pions deposited their energy in that case primarily in the five calorimeter towers they encountered along the shower axis: The towers numbered 17, 6, 1, 3 and 11. In the 90° geometry, the shower axis traversed the same towers in the opposite direction: Towers 11, 3, 1, 6 and 17, respectively.

At $\phi = 90°$, the total thickness of the calorimeter was 36 cm, or $1.8\lambda_{\mathrm{int}}$, and each of the five towers traversed by the shower axis was $0.36\lambda_{\mathrm{int}}$ thick. At an angle of 24°, the path of the shower axis through each of the mentioned towers had a length of $72\,\mathrm{mm}/\sin 24° = 177\,\mathrm{mm}$, or $0.885\lambda_{\mathrm{int}}$. In first approximation, the signals from the mentioned towers thus represented 5 longitudinal segments with a depth of $0.885\lambda_{\mathrm{int}}$ each, $4.43\lambda_{\mathrm{int}}$ in total. However, reality was somewhat more complicated.

6.2.1. Impact point dependence

Beam particles entering the detector in the copper layer separating two horizontal fiber layers encountered essentially only copper during the early stage of their shower development. For all practical purposes, the first longitudinal segment was thus thicker than average for such showers. In the 24° geometry, the first longitudinal segment was Tower 17. If this tower were made of massive copper, then its effective depth would be $\frac{177}{151} = 1.17\lambda_{\mathrm{int}}$, instead of the average value of $0.885\lambda_{\mathrm{int}}$. Similarly, the effective thickness of this first segment would be less than average for particles entering the detector in the "Swiss cheese" part, i.e., in the horizontal fiber layers: $0.72\lambda_{\mathrm{int}}$.

Particles entering the calorimeter in the horizontal fiber planes thus deposited a smaller fraction of their total energy in Tower 17 than did particles entering in the copper. However, in the deeper calorimeter segments, beyond the shower maximum, the situation was reversed. Particles entering the calorimeter in the fiber planes penetrated, on average, deeper inside before undergoing the first nuclear interaction that started the shower development. As a result, they deposited more energy and generated larger signals in these deeper segments than the pions that entered the calorimeter in a copper layer that separated the fiber planes.

This is illustrated in Fig. 9, which shows the average scintillator signals measured in the different towers located on the shower axis of 200 GeV π^- traversing the

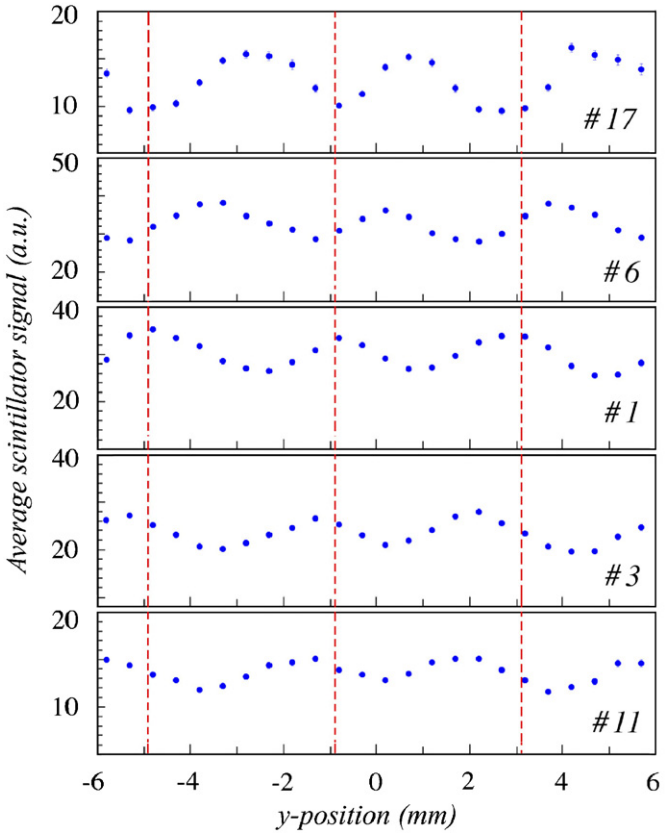

Fig. 9. Average (scintillator) signals observed in towers traversed by 200 GeV π^- entering the calorimeter at an angle of 24° with the fiber axis, as a function of the y-coordinate of the impact point of the particles. The dashed vertical lines correspond to positions where the particles entered the calorimeter in a horizontal fiber plane. See Fig. 3 for geometric details.

calorimeter at 24°. These average signals are plotted as a function of the y-coordinate of the impact point of the pions. The dashed vertical lines indicate the y-positions of the fiber planes, separated by 4 mm. The signals in the first tower seen by the particles (#17) reach a minimum at these positions, while the signals in the deeper towers (in particular #1 and #3) reach their maximum values there. Comparing the patterns in Towers 1, 3 and 11, it seems as if the maximum signals are gradually drifting towards smaller y-values. This could indicate that the detector was not positioned completely level during these measurements. A tilt of ~0.2° would be enough to produce the observed drift of 1 mm over a distance of 30 cm.

By separating the events into subsamples according to the y-coordinate of their impact point, we doubled the number of measurement points on the longitudinal shower profile, from 5 to 10. Once the pion shower had started, the effective difference in the thickness of the absorber resulting from the impact point vanished. And since this starting point was most likely located in the first calorimeter segment, the differences in effective thickness were largest in that segment.

The situation was somewhat more complicated in the case of the 90° data. Here, the effective thickness of a calorimeter tower amounted, on average, to $0.36\lambda_{\rm int}$. For particles that entered the detector in a copper layer, the effective tower thickness was $0.47\lambda_{\rm int}$ until they interacted with a nucleus and started a shower. On the other hand, the effective tower thickness for particles entering in a fiber plane was only $0.29\lambda_{\rm int}$. In the latter case, the total thickness of the calorimeter, for non-showering particles, was thus only $1.5\lambda_{\rm int}$. Therefore, a significant fraction of the pions traversed the entire detector without starting a shower. The mean free path of a high-energy pion is larger than that for protons, which forms the basis of the definition of the nuclear interaction length. Typically, $\lambda_\pi \approx 1.5\lambda_{\rm int}$ [15]. Therefore, the "punch-thru" probability for high-energy pions amounted to $\exp(-1.5/1.5)\sim 37\%$ when they entered the calorimeter in a fiber plane. For pions entering in the copper separating fiber planes, the probability of traversing the calorimeter without starting a shower was smaller: $\exp(-5\times 0.47/1.5)\sim 20\%$.

This phenomenon is illustrated in Fig. 10, which shows the fraction of particles that produced a total signal smaller than 2 mip in the calorimeter, as a function of the y-coordinate of the impact point. This fraction oscillates with a period of 4 mm, the size of the copper tubes of which the detector is made. The maximum and minimum punch-thru probabilities are approximately equal to the values calculated above, which supports our assessment of the mean free path of the beam pions. We calculated the effective thicknesses of the different calorimeter towers in this geometry by taking into account the punch-thru probability. For example, a pion that entered the calorimeter in a fiber plane had a probability of 80% to penetrate the first tower (#11) without starting a shower. Therefore, the effective thickness of this tower was taken to

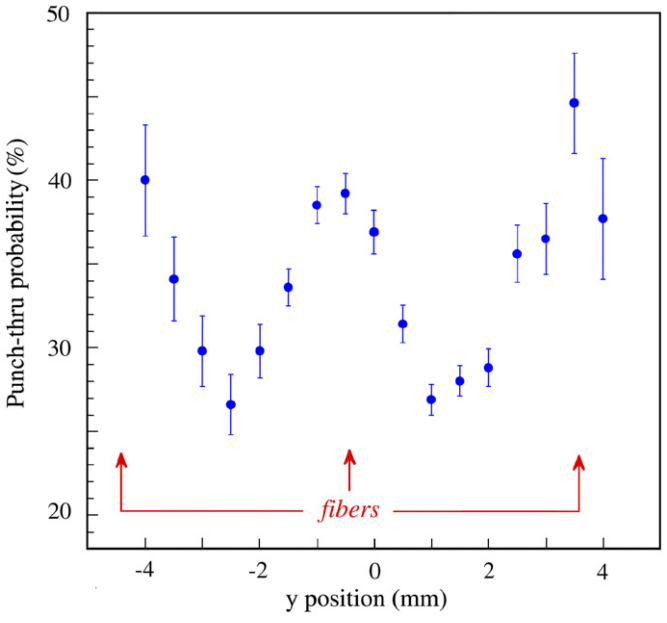

Fig. 10. Fraction of non-showering particles as a function of the y-coordinate of the impact point of the particles. Data for 100 GeV π^+ entering the calorimeter at $\phi = 90°$.

be $0.80 \times 0.29 + 0.20 \times 0.36 = 0.30\lambda_{int}$. The probability that the pion also traversed the second tower (#3) without starting a shower was 66%, therefore the effective thickness of this tower was $0.66 \times 0.29 + 0.34 \times 0.36 = 0.31\lambda_{int}$, etc. The same method was used to calculate the effective thicknesses of the towers in the $\phi = 24^\circ$ geometry.

All the above information is summarized in Table 3, which lists the sections of the longitudinal profile sampled by the various towers for the 24° and 90° event samples. The average depth of each section is given in parentheses.

6.2.2. Longitudinal profile results

Longitudinal profiles measured with the Cherenkov signals are shown in Fig. 11, for pions in the energy range from 20 to 300 GeV that entered the calorimeter at $\phi = 24^\circ$. This figure shows the typical, well known shower characteristics: A relatively steep rise to the shower maximum, followed by a more or less exponential decrease. The shower maximum shifts gradually to greater depths with the pion energy, from $\sim 1.3\lambda_{int}$ at 20 GeV to $\sim 2\lambda_{int}$ at 300 GeV. The exponential decrease beyond the shower maximum is similar for all shower energies. It should be emphasized that the profiles shown in Fig. 11 were derived on the basis of the signals from the towers located on the shower axis, i.e., the numbered towers from Fig. 3. Especially beyond the shower maximum, a significant fraction of the shower energy was deposited in other towers as well.

However, as in the case of the lateral shower profiles, the main purpose of these measurements was not so much a detailed study of the longitudinal shower development itself, but rather of *differences* between the profiles measured with the two types of signals generated by this instrument. Fig. 12a shows the average Cherenkov and scintillator signals as a function of depth, for 100 GeV π^+ entering the detector at 90° with the fiber direction. Clearly, in this geometry only the early part of the developing shower is probed, up to and maybe a little beyond the shower maximum. The Cherenkov signals were considerably smaller than the scintillator ones. This is shown in more detail in Fig. 12b, which gives the ratio between the two signals as a function of depth. The full circles correspond to the towers located on the shower axis, i.e., Towers 11, 3, 1, 6 and 17, respectively. As for the profiles themselves (Fig. 12a), each of these towers provided two data points, because of the splitting of the event samples according to impact point.

Early in the shower, the Cherenkov signals were, on average, a factor of 4–5 smaller than the scintillator ones. However, as the shower developed, the difference became less pronounced. Near the shower maximum, the difference was about a factor of two. A similar tendency, even more pronounced, was observed for the signals measured in off-axis towers (the triangles in Fig. 12b), for which we used

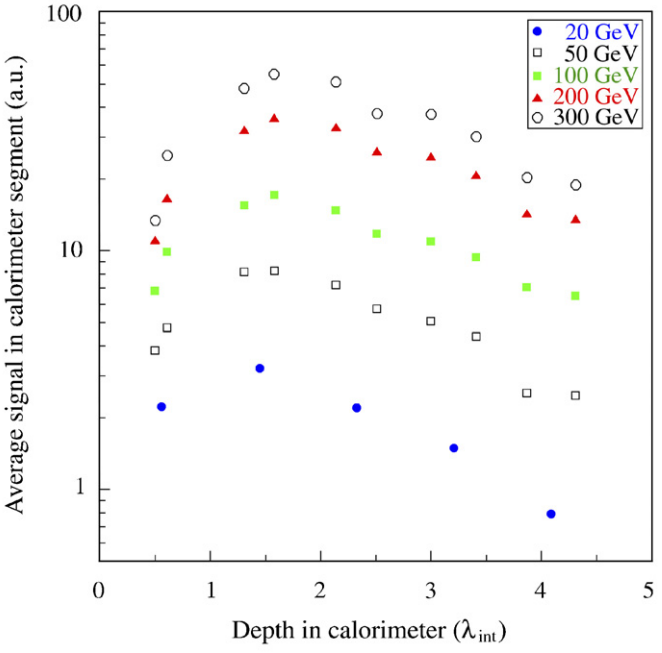

Fig. 11. Comparison of the longitudinal shower profiles for pions of energies ranging from 20 to 300 GeV, measured with the Cherenkov signals.

Table 3
The effective depth range and (in parentheses) the average depth, given in nuclear interaction lengths, of the various longitudinal segments of the DREAM calorimeter, for event samples with different impact points

Impact point, 24°	Tower 17	Tower 6	Tower 1	Tower 3	Tower 11
Fiber plane	0.1–0.89	0.89–1.72	1.72–2.56	2.56–3.43	3.43–4.30
	($0.50\lambda_{int}$)	($1.31\lambda_{int}$)	($2.14\lambda_{int}$)	($3.00\lambda_{int}$)	($3.87\lambda_{int}$)
Cu plane	0.1–1.11	1.11–2.05	2.05–2.96	2.96–3.86	3.86–4.75
	($0.61\lambda_{int}$)	($1.58\lambda_{int}$)	($2.51\lambda_{int}$)	($3.41\lambda_{int}$)	($4.31\lambda_{int}$)
Impact point, 90°	Tower 11	Tower 3	Tower 1	Tower 6	Tower 17
Fiber plane	0.05–0.35	0.35–0.67	0.67–0.99	0.99–1.32	1.32–1.65
	($0.20\lambda_{int}$)	($0.51\lambda_{int}$)	($0.83\lambda_{int}$)	($1.16\lambda_{int}$)	($1.49\lambda_{int}$)
Cu plane	0.05–0.49	0.49–0.91	0.91–1.31	1.31–1.70	1.70–2.08
	($0.27\lambda_{int}$)	($0.70\lambda_{int}$)	($1.11\lambda_{int}$)	($1.51\lambda_{int}$)	($1.89\lambda_{int}$)

The top table concerns the measurements performed at $\phi = 24^\circ$, the bottom table is for $\phi = 90^\circ$. See text for details.

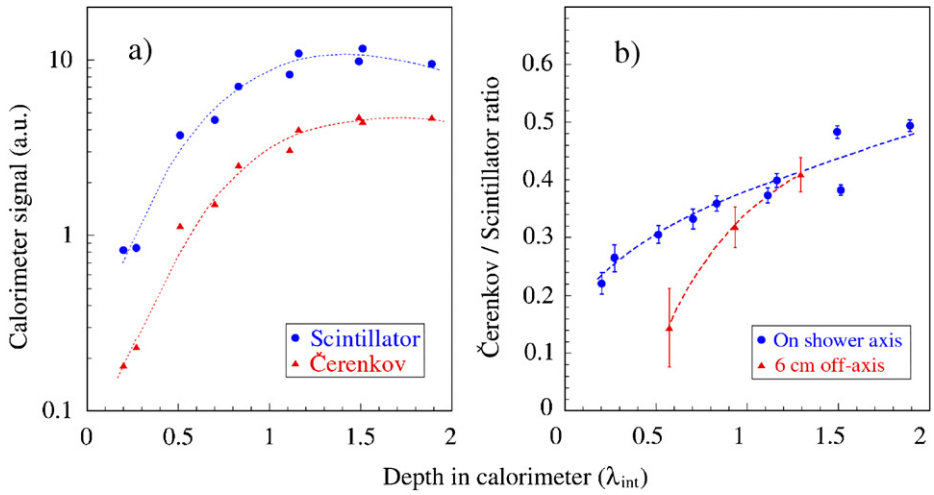

Fig. 12. The average Cherenkov and scintillator signals from 100 GeV pion showers as a function of depth, for particles entering the detector at an angle $\phi = 90^\circ$ with the fiber direction. These signals concern the towers located on the shower axis (a). The ratio of both signals as a function of depth, measured separately for towers located on the shower axis and for towers whose center was located at a distance of 6 cm from the shower axis (b). All lines are drawn to guide the eye.

the sum of the signals observed in Towers $10+12$, $2+4$, $7+5$ and $18+16$, respectively (see Fig. 2). No distinction on the basis of impact point was made in this case. These signals were extremely small, especially early in the shower, hence the large error bars (which are dominated by pedestal fluctuations for these data points).

These effects are not dissimilar from those observed for electromagnetic showers in the same geometry [9]. The reason for the strong suppression of the Cherenkov response is the fact that Cherenkov light is directional, it is emitted at a characteristic angle (of $\sim 46^\circ$) by the superluminous shower particles (see also Section 5). The collimated early component of em showers is strongly dominated by shower particles traveling in the same direction as the particle that caused the shower. If that particle travels perpendicular to the fiber axes, then the Cherenkov light falls outside the numerical aperture of the fibers. As the em shower develops, and especially beyond its shower maximum, Compton electrons become an increasingly dominating source of Cherenkov light. And since these electrons are, in first approximation, emitted isotropically with respect to the direction of the shower axis, the Cherenkov response, and thus the ratio of the Cherenkov and scintillator signals increases.

The off-axis towers have the additional characteristic that energy deposited there comes from particles that must have traveled at a considerable angle with the shower axis, since they would otherwise never have reached these towers. Early in the shower, only non-relativistic particles (in particular neutrons produced in nuclear reactions, which do produce scintillation through elastic scattering off the protons in the plastic scintillator, but no Cherenkov light) dominate the signals, but deeper inside π^0s traveling at a significant angle with the shower axis may contribute as well. As indicated in Fig. 5, the Cherenkov response to such π^0s may be significantly larger than the scintillator response, especially in the towers equipped with quartz fibers. These phenomena are most likely responsible for the fact that the observed Cherenkov/scintillator ratio in the off-axis towers increases faster with depth than for the towers on the shower axis.

Quantitatively, the observed Cherenkov/scintillator ratios in the on-axis towers are also as expected. In the 0° geometry, we measured the ratio of the Cherenkov and scintillator signals from 100 GeV pions to be 0.78 [3]. Fig. 5 shows that the response to the em shower component (which is almost entirely responsible for the Cherenkov signals) decreases by a factor of three when the detector is rotated from 0° to 90°. Since the scintillator response is independent of the angle of incidence of the particles, one should thus expect the 90° Cherenkov/scintillator ratio in the early stages of the shower development to be $0.78/3 = 0.26$, in good agreement with the observations.

The Cherenkov/scintillator ratios measured for the 24° geometry can be understood on the basis of similar considerations. The experimental results are shown in Fig. 13, both for on-axis and off-axis towers, as before. In this geometry, the Cherenkov/scintillator signal ratio for the on-axis towers is actually *larger* than that for the 0° geometry in which the detector was calibrated. This is commensurate with the angular response for em showers measured at this angle of incidence [9] (see also Fig. 5) and can be understood from the fact that the early, collimated component of em showers partially falls within the numerical aperture of the fibers.

As in the case of the lateral profiles, the precise extent of these effects is very sensitive to the numerical aperture of the fibers, which was different for the towers in the Outer Ring and the rest of the calorimeter (Section 2). According to Fig. 5, the Cherenkov response of an em shower in a DREAM calorimeter equipped with plastic fibers increases by $\sim 60\%$ when the angle of incidence is increased from 0°

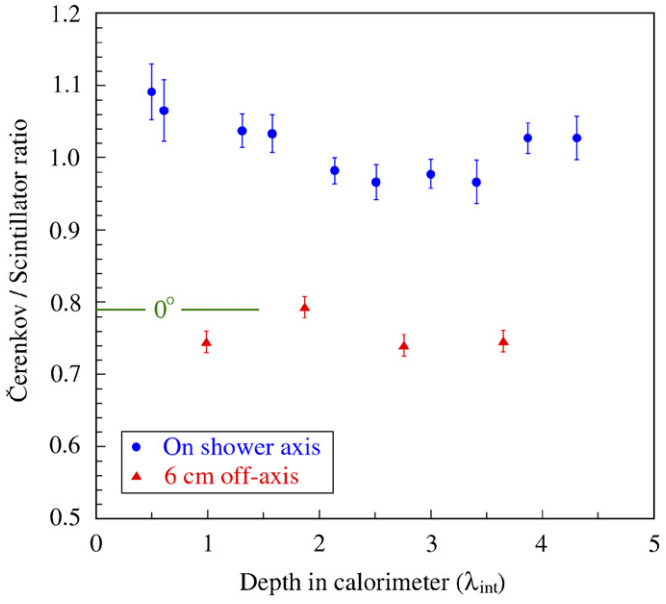

Fig. 13. Ratio between the average Cherenkov and scintillator signals from 200 GeV pion showers as a function of depth. The pions entered the detector at an angle $\phi = 24^\circ$ with the fiber direction. Results are given separately for the calorimeter towers located on the shower axis (full circles) and for towers whose center was located at a distance of 6 cm from the shower axis (triangles). The horizontal line labeled 0° represents the Cherenkov/scintillator signal ratio for 200 GeV pions at $\theta = 0$, the orientation at which the signals were calibrated with electrons.

to 24°. For the quartz fibers, the increase is somewhat smaller, ~40%. Since the 24° is close to the boundary at which the component that is parallel to the shower axis falls within the acceptance of the Cherenkov fibers, the actual increase will be somewhat smaller for hadron showers. This is because the π^0s (responsible for the bulk of the Cherenkov signal) are produced at some angle with the direction of the incoming hadron, which leads to smearing effects in the angle between the em shower axes and the fibers.

It is interesting to note that the experimental data show indeed that the Cherenkov response to hadrons entering the calorimeter at an angle of 24° is largest for the first (#17) and last (#11) of the five towers on the shower axis. These towers were equipped with plastic Cherenkov fibers. The response was smaller for Towers 6, 1 and 3, which were equipped with quartz fibers. The increase of the Cherenkov/scintillator signal ratio with respect to the 0° case was, on average, 38% for Tower 17 and 25% for the quartz towers. For the off-axis towers, the off-axis Cherenkov/scintillator ratio was not very different from the 0° one. This difference between the on-axis and off-axis results reflects the difference in the lateral profiiles described in Section 6.1: as the radial distance increases, the Cherenkov/scintillator ratio decreases, especially in towers equipped with plastic fibers (see Fig. 7).

6.2.3. Longitudinal shower containment

As in the case of the lateral profiles, the measured longitudinal profiles make it possible to estimate the shower leakage or, more precisely, the fraction of the total signal that would have been generated in an infinitely deep calorimeter of this type that is missed because of the finite dimensions of the instrument. As in the case of the lateral leakage, this fraction is not necessarily the same for the two types of signals.

To assess the longitudinal leakage, it was not sufficient to limit the analysis to the towers located on the shower axis. Deep inside the detector, the showers were considerably broader than one tower and, therefore, the off-axis towers were very important for this assessment. Fig. 14 shows longitudinal shower profiles measured for 100 GeV π^- in the 24° geometry, for the shower axis (Towers 17,6,1,3,11), for an axis located at a radial distance of 6 cm (Towers 18 + 16, 7 + 5, 2 + 4, 10 + 12) and for an axis located at a radial distance of 12 cm (Towers 19 + 15, 8 + 14, 9 + 13, see Fig. 2). The figure shows that the shower maximum moves gradually to greater depth as one moves away from the shower axis. Beyond the shower maximum, the profile measured on the shower axis exhibits the exponential decrease already observed before. We assume that the off-axis profiles decrease similarly beyond their respective shower maxima. Based on this assumption, for which experimental evidence is lacking, we have estimated the shower leakage outside the active calorimeter volume. In the case of the scintillator signals from 100 GeV π^-, the total leakage found in this way was ~20%, with approximately equal contributions from the on-axis and off-axis towers. We repeated the same analysis for pions of

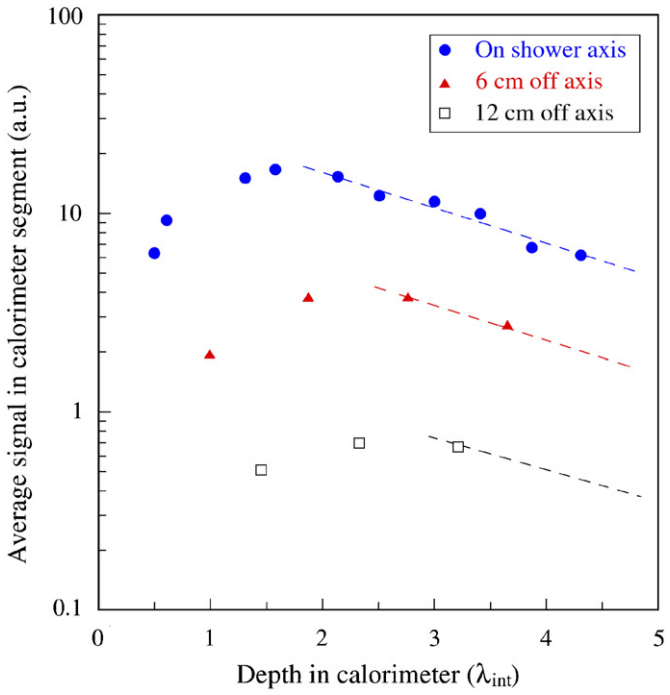

Fig. 14. Longitudinal shower profile for 100 GeV π^- entering the calorimeter at an angle of 24° with the fiber axis. Shown are the profiles measured on the shower axis and at two different distances from the shower axis, from the scintillator signals. The dashed curves indicate the profiles assumed for the calculation of shower leakage.

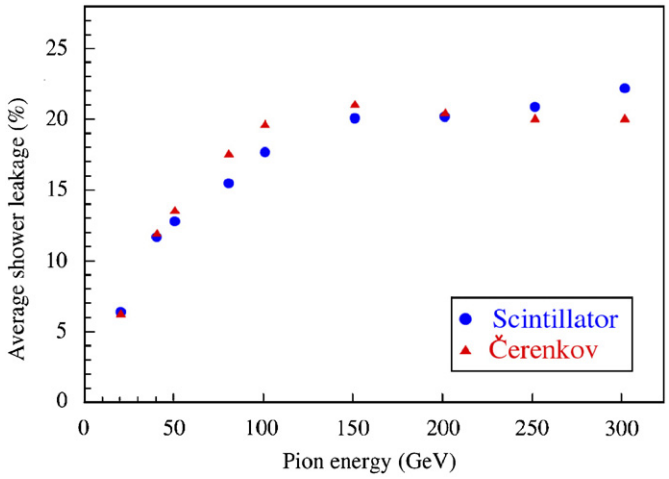

Fig. 15. Longitudinal shower leakage as a function of the energy of showering pions, in the 24° geometry (effective calorimeter depth $4.5\lambda_{int}$). Results are given as a fraction of the total signal in an infinitely large calorimeter, separately for scintillation and Cherenkov light.

other energies. Fig. 15 shows the average leakage fraction as a function of energy, for the two types of calorimeter signals, for the 24° geometry. This fraction ranged from ~6% at the lowest energy (20 GeV) to ~22% at 300 GeV. The figure shows that differences between the two types of signals are small, and much less evident than for the lateral shower leakage. This is because the spatial separation between the relativistic and non-relativistic shower particles is much less evident in the longitudinal direction than in the lateral plane. At a depth of $10\lambda_{int}$ or more, non-relativistic shower particles are possibly a dominating component, resulting in differences between scintillator and Cherenkov signals. However, in the (limited) longitudinal range covered by our studies, production of π^0s is very prominent and dominating the signals. At an angle of 24°, the calorimeter is simply not deep enough to see significant evidence of the contributions of non-relativistic shower particles.

7. Conclusions

We have measured lateral and longitudinal hadronic shower profiles in a copper-based calorimeter equipped with two active media. Scintillating fibers measured the energy deposit profile, while clear fibers measured the profile of the shower particles capable of generating Cherenkov light. We observed the following features:

- The Cherenkov showers are considerably narrower than the energy deposit profile. This is because the halo consists in large part of non-relativistic shower particles, mainly protons. The detector volume needed to collect at least 95% or 99% of the total shower signal is more than 50% larger for the scintillation light (see Table 2).
- The Cherenkov signals from the early stage of the developing hadron showers are very sensitive to the orientation of the fibers. Since many of the shower particles that generate the Cherenkov signals are traveling in approximately the same direction as the beam, these signals may be suppressed by as much as a factor of five, or enhanced by up to 40% (compared with the scintillator signals), depending on the angle of incidence of the beam with respect to the fiber direction (see Figs. 12b, 13).
- Beyond the shower maximum, the dependence of the Cherenkov/scintillator signal ratio on the fiber orientation rapidly vanishes if one moves away from the shower axis. This may be concluded from a comparison of Figs. 12b and 13.
- Differences between the two types of signals become gradually less pronounced as the shower develops longitudinally (see Fig. 12). It should be kept in mind, though, that energetic π^0 are abundantly produced close to the shower axis, at depths well beyond the shower maximum [16]. Therefore, the enhancement of the Cherenkov signal observed for angles of incidence of ~20° (at which Cherenkov light emitted by the beam particles falls within the numerical aperture of the fibers) is still observed at depths of more than $4\lambda_{int}$ (see Fig. 13).
- The detector volume needed for longitudinal containment did not measurably depend on the type of signal (see Fig. 15).

Acknowledgments

We gratefully acknowledge the contributions of Tracy McAskill, Vladimir Nagaslaev, Alan Sill, Veronica Stelmakh, Yunyong Wang, Erika Washington and Kim Zinsmeyer to the construction of the DREAM detector. We thank CERN for making particle beams of excellent quality available. Our beam tests would not have been possible without the help we received from Claude Ferrari and Maurice Haguenauer. We thank K. Kuroda for loaning us the fiber hodoscopes, and A. Gorin and I. Manouilov for their assistance with the data acquisition system. This study was carried out with financial support of the United States Department of Energy, under contract DE-FG02-95ER40938, and the Advanced Research Program of the State of Texas.

References

[1] R. Wigmans, Calorimetry—Energy Measurement in Particle Physics, International Series of Monographs on Physics, vol. 107, Oxford University Press, 2000.
[2] N. Akchurin, et al., Nucl. Instr. and Meth. A 536 (2005) 29.
[3] N. Akchurin, et al., Nucl. Instr. and Meth. A 537 (2005) 537.
[4] N. Akchurin, et al., Nucl. Instr. and Meth. A 533 (2004) 305.
[5] D. Acosta, et al., Nucl. Instr. and Meth. A 316 (1992) 184.
[6] H. Abramowicz, et al., Nucl. Instr. and Meth. 180 (1981) 429.
[7] M.G. Catanesi, et al., Nucl. Instr. and Meth. A 260 (1987) 43.
[8] P. Amaral, et al., Nucl. Instr. and Meth. A 443 (2000) 51.

[9] N. Akchurin, et al., Nucl. Instr. and Meth. A 548 (2005) 336.
[10] N. Akchurin, R. Wigmans, Rev. Sci. Instr. 74 (2003) 2955.
[11] O. Ganel, R. Wigmans, Nucl. Instr. and Meth. A 365 (1995) 104.
[12] F. Barreiro, et al., Nucl. Instr. and Meth. A 292 (1990) 259.
[13] N. Akchurin, et al., Nucl. Instr. and Meth. A 399 (1997) 202.
[14] F. Binon, et al., Nucl. Instr. and Meth. 206 (1983) 373.
[15] D. Acosta, et al., Nucl. Instr. and Meth. A 305 (1991) 55.
[16] D. Green, in: Proceedings of the Fourth International Conference on Calorimetry in High Energy Physics, La Biodola, Italy, in: A. Menzione, A. Scribano (Eds.), World Scientific, Singapore, 1994, p. 1.